Electrically Active Screw Dislocations in Helical ZnO and Si Nanowires and Nanotubes

Evgeniya Akatyeva,[†] Liangzhi Kou,[‡] Ilia Nikiforov,[†] Thomas Frauenheim,[‡] and Traian Dumitrică[†,*]

[†]Department of Mechanical Engineering, University of Minnesota, Minneapolis, Minnesota 55455, United States and [‡]BCCMS, Universität Bremen, Bremen 28359, Germany

ABSTRACT While the presence of axial screw dislocations in helical nanowires and nanotubes is known to be due to the growth process, their effect on the electronic properties remains unexplored. Relying on objective molecular dynamics simulations coupled to density functional tight-binding models for ZnO and Si, and supporting density functional theory calculations, we predict significant screw-dislocation-induced band gap modifications in both materials. The effect originates in the highly distorted cores and should be present at radii larger than those considered in our simulations (maximum ~2 nm) as well as in other materials. The observed band gap dependences on the size of the Burgers vector and wall thickness could motivate new strategies for growing, *via* the screw dislocation mechanism, stable nanostructures with desired band gaps.

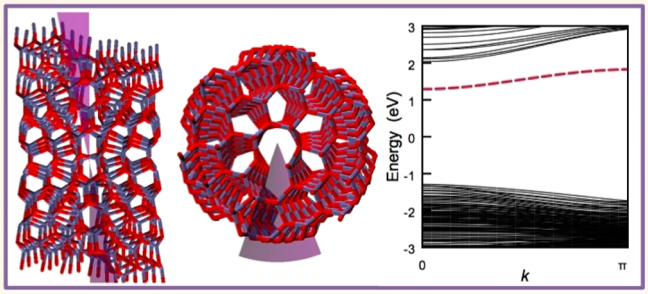

KEYWORDS: nanowires · nanotubes · screw dislocations · Eshelby twist · electrical properties · objective molecular dynamics

Due to their intrinsic one-dimensionality combined with quantum confinement effects, semiconductor nanowires (NWs) and nanotubes (NTs) exhibit novel electronic and optical properties, of interest for various nanoscale device applications. An understanding of the structure−electronic properties relationship is crucial for advancing these applications. Screw dislocations are an important type of extended defect identified in a variety of quasi-one-dimensional materials including PbS, GaN, PbSe, ZnO, In_2O_3, InP, Cu_2O, CdS, and CdSe[1−11] NWs and NTs. The reason for an axial screw dislocation to exist in these nanostructures is known to be its involvement in the growth processes.[1−6,8−11] What is less known is the structure−electronic properties relationship in these novel organizations of matter. This represents a challenging endeavor not only because of the small scale involved but also because the axial screw dislocation couples to the shape of NWs and NTs.[1−11]

On the basis of macroscopic elastic theory, Eshelby predicted that a whisker containing a screw dislocation exhibits a stabilizing torsional deformation,[11−13] which depends directly on the magnitude of the Burgers vector b and inversely on the cross-sectional area πR^2; $\gamma_E = b/\pi R^2$. Interestingly, all the experimentally observed NWs and NTs containing axial screw dislocations were twisted, prompting comparisons[1,4,5,7] with the Eshelby model originally developed for the much larger scale. Nevertheless, the measured[7] twist rate was sometimes found to be only in semiqualitative agreement with γ_E.

In a broader view, it is unclear if any disagreement between experiment and the continuum model should be attributed to a possible invalidation of the classical continuum model by the presence of surface effects or to the extraordinary challenges associated with measuring the atomic scale twist. While quantum mechanical microscopic modeling could shed light onto this aspect, there are challenges associated not only with the accurate description of chemical bonding but also with a quantum mechanical description of large systems. Indeed, with standard methods, one can efficiently simulate only ideal NWs and NTs by considering their translational periodicity **T** and accounting for the small number of atoms *N* located in one primitive cell. Unfortunately, the generated twist (unknown

* Address correspondence to dtraian@me.umn.edu.

Received for review August 17, 2012 and accepted October 9, 2012.

Published online October 09, 2012
10.1021/nn303747c

beforehand) prevents the applicability of the standard periodic boundary conditions (PBC) treatment.

The technique used here—objective molecular dynamics[14] (MD)—is able to overcome the large-size difficulty. Without introducing any additional approximations, it allows for performing atomistic simulations of screw-dislocated NWs and NTs in an economic fashion, using the same N atoms located in the primitive translational cell prior to the introduction of the dislocation. The infinitely long NWs and NTs are described as objective structures,[15] with

$$\mathbf{X}_{j,\zeta} = \mathbf{R}^{\zeta}\mathbf{X}_j + \zeta\mathbf{T}, j = 1, ..., N; \ -\infty < \zeta < \infty \quad (1)$$

Here, $\mathbf{X}_{j\zeta}$ and $\mathbf{X}_j$ represent the Cartesian coordinates of atoms j located in the cell labeled by integer ζ and initial cell, respectively. Matrix $\mathbf{R}$ indicates a rotation with angle θ around the direction indicated by vector $\mathbf{T}$, here taken along the z-axis. In objective MD, only the N atoms in the initial cell are explicitly simulated under the objective boundary conditions indicated by eq 1. We coupled eq 1 with the two-center nonorthogonal symmetry-adapted tight binding[16] in the code Trocadero.[17] The electronic states are represented in terms of generalized Bloch sums

$$|j\alpha, k\rangle \propto \sum_{\zeta} e^{ik\zeta} |j\alpha, \zeta\rangle, \ -\pi < k \leq \pi \quad (2)$$

where α indicates the symmetry of a valence atomic orbital located on atom j, and k is the helical wavenumber. Note that the above scheme gives the entire electronic spectrum as a function of k, instead of the usual wavevector k encountered in solid-state physics.

Concerning the description of the chemical bond, density functional-based potentials[18,19] are known to give accurate and computationally efficient descriptions of chemical bonding in zinc compounds and silicon. Relying on objective MD coupled with symmetry-adapted non-orthogonal tight-binding and density functional-based potentials, in this paper we investigate whether the presence of the screw dislocation has any effect on the electronic properties of nanostructures. The main results were further verified with full density functional theory (DFT) calculations and local density approximation calculations with d orbital correction (LDA+U).

Modulating the electronic structure of semiconducting NWs and NTs presents great importance for device applications, as these structures have been proposed as important components in electronic and optoelectronic nanodevices. To achieve this goal, several possibilities are investigated including change in quantum confinement by diameter variations and orientations,[20] doping with impurities,[21] and surface doping.[22−24] Uniaxial and biaxial strain variations were also shown to significantly affect the electronic properties of semiconducting nanoribbons and nanomembranes.[25−28] Along this latter line of research, here we identify a new way to influence the electronic band structure at the nanoscale, *via* the high strain generated at the core of an axial screw dislocation. The robustness of the effect is demonstrated in calculations performed on two important semiconducting nanomaterials, ZnO and Si, which already found many applications including photonics[29] and solar energy conversion.[30,31] So far, classical investigations of dislocations in the bulk[32,33] were conducted mainly from the perspectives of the dislocation-induced gap states and band bending of the bulk due to the presence of such states. Here we pursue an investigation from a microscopic and nanoscale level viewpoint and propose a new utility.

RESULTS AND DISCUSSION

We simulated a large set of pristine and screw-dislocated ZnO NWs and NTs with a wurtzite structure and of H-passivated Si NWs with a cubic diamond structure. Our ZnO NWs have an initial translational periodicity of 5.32 Å along the [0001] direction and are bound by six nonpolar $\{10\bar{1}0\}$ surfaces, which are the most stable surfaces in ZnO. In comparison with other surfaces, the ZnO dimers located on $\{10\bar{1}0\}$ are known to exhibit significant relaxation[34−36] but not reconstruction. The number of layers L in the cross section was varied from 2 to 6, such that their radii, as defined in ref 37, varied from 5.5 to 17.7 Å. Next, from each pristine L NW we created a set of (L,h) NTs, by systematically removing inner atomic layers. We label by h the number of missing layers. Finally, in all these structures we introduce screw dislocations with the axis at the center and minimal Burgers vectors b = 5.4 Å in NWs and larger (multiple of b) in NTs. For this, we used the morphologies of the pristine relaxed structures. Starting from the center, the atoms in the vicinity of the cut-plane were gradually displaced along the dislocation axis until atomic displacements equal to the magnitude of the desired Burgers vector were reached and maintained up to surface atoms. Note that the chosen location of the dislocation axis is not crossing any atomic site. In Si, we considered ⟨110⟩ NWs exhibiting hexagonal cross sections. The number of $\{111\}$ layers in the cross section was varied from 6 to 12 in steps of 2 so that the radii of the created NWs ranged from 6.27 to 18.8 Å. The surface region is expected to be electrically active due to the undercoordinated Si atoms. Since we are interested in elucidating the effect of the screw dislocation, all these surface states were suppressed by passivating with H each Si dangling bond located on the surface. We introduced "shuffle"-type screw dislocations with the Hornstra core[38] located at the NW center and the minimal Burgers vector b = 3.8 Å.

Because the number of atoms N in the primitive objective motif is independent of the values of the structural parameters, adoption of helical symmetry (1) enables systematic calculations of chiral and twisted NWs and NTs[37−41] that would otherwise be beyond

reach. With the symmetry-adapted treatment of the electronic states (2), conjugate gradient structural relaxations can be carried out with the structural parameters |**T**| and θ taking arbitrary values. The obtained potential energy surface indicated that even for the smallest structures (see Table 1, referring to the ZnO study) the optimized structural parameters, as well as the inner and outer radii, are close (within ±3%) to the values predicted from the bulk. The derived surface energy values σ_s are found to be in good agreement with the *ab initio* DFT value of 64.3 meV/Å^2 for the $\{10\bar{1}0\}$ surface.[34−36] These conclusions are further supported by our full DFT calculations performed on the selected structures, summarized as well in Table 1. At the larger considered diameters, the differences with bulk were even less notable as the perturbation caused by the surface relaxation becomes less significant.

TABLE 1. Geometric Characteristics, Energetics, and Band Gaps of the DFTB-Optimized Pristine ZnO (L,h) NWs and NTs[a]

(*L*,*h*)	|T| (Å)	ε (%)	*R* (Å)	ε* (%)	*r* (Å)	E_f (eV/Å)	σ_s (meV/ Å^2)	band gap (eV)
(2,0)	5.44	2.3	5.49	−2.4	0	2.42	70.2	3.27
(3,0)	5.39	1.5	8.53	−1.2	0	3.64	67.9	3.29
(3,1)	5.44	2.4	8.61	−0.3	2.60	4.64	65.9	3.32
(3,0)[b]	5.36	0.8	8.56	−0.8	0	3.09	57.5	1.17 (2.45[c])
(3,1)[b]	5.42	1.9	8.55	−1.0	3.2	5.09	68.9	1.40 (2.42[c])
(4,0)	5.37	1.1	11.57	−0.7	0	4.86	66.8	3.31
(4,1)	5.40	1.5	11.62	−0.3	2.60	5.94	66.5	3.30
(4,2)	5.45	2.5	11.70	0.4	5.65	6.89	63.3	3.33
(4,0)[b]	5.36	0.8	11.40	−2.1	0	5.01	69.8	0.89

[a] ε and ε* are the axial and radial (outer radius only) pre-strains, as measured with respect to the bulk material. E_f and σ_s are the formation (measured from bulk) and surface energies, respectively, related by $E_f = 2\pi\sigma_s(R+r)$. [b] Results obtained with DFT. [c] These band gap values were obtained with LDA+U.

All objective MD simulations indicated that the pristine NWs and NTs cut from the bulk did not possess intrinsic twists. However, in all screw-dislocated structures the optimal angular parameter θ_E is nonzero in the stress-free state. Examples of such calculations are shown in Figure 1, plotting the total energy of the pristine, Figure 1a, and screw-dislocated (3,0) ZnO NW *versus* θ, Figure 1b. While the pristine NW has a minimum at θ = 0° (*i.e.*, the stress-free structure is untwisted), the screw-dislocated NW exhibits a minimum at θ_E = 6.7° corresponding to an intrinsic twist rate of γ_E = 1.26°/Å. Note also that in the untwisted NW the DFTB formation energy of the dislocation of 1.88 eV/ Å compares well with the full DFT value of 1.61 eV/ Å and, thus, indicates reliability of the DFTB modeling.

Our data for ZnO summarized in Table 2 show that the amount of microscopic twist has a complex dependence on the parameter space, *r*, *R*, and b. Nevertheless, our previous comprehensive analysis[37,38,41] of the morphologies of these relaxed structures elucidated that in both ZnO and Si the amount of twist and dislocation energies can be rationalized with Eshelby's twist model supplemented by a nonlinear-elastic energy term.

The dislocation core, which cannot be treated with the linear elasticity, is the highly distorted central

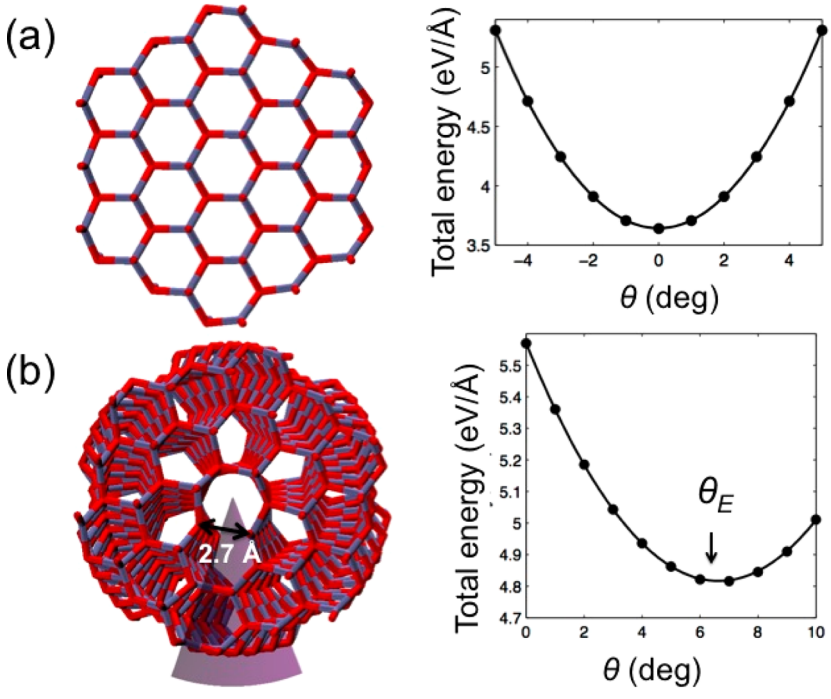

Figure 1. Atomistic representation of DFTB stress-free configuration (left) and total energy *vs* twist angle (right) for (a) (3,0) and (b) (3,0)$_b$ ZnO NW with *R* = 8.53 Å. The twisted purple plane indicates the cut made to create the dislocation. The angle at the minimum gives the Ehelby twist $\gamma_E = \theta_E/|T_E|$.

region close to the dislocation axis. It has an estimated radius ranging from one to five Burgers vectors. Outside the core, deformation is less dramatic and linear elasticity works very well.[37,38] In the center of the relaxed ZnO NWs we identified broken Zn−O bonds and new homoelemental Zn−Zn and O−O interactions. For instance, in the DFTB relaxed screw-dislocated $(3,0)_b$ ZnO NW shown in Figure 1b, the length of originally connected 2.0 Å axial Zn−O bonds became 3.3 Å long. The smallest distances between Zn−Zn and O−O atoms in the core region are 2.8 and 2.7 Å, respectively. Note that even the open-core NTs can contain Zn−Zn and O−O atom pairs at these distances when the Burgers vector is large enough, such as in the $(6,1)_{3b}$ case. In the DFTB relaxed pristine NW, these Zn−Zn and O−O distances measure 3.28 Å. In Si NWs, the considered Burgers vector is smaller in size. For this reason, in the relaxed structures, the set of Si−Si bonds adjacent to the dislocation axis stay connected, although they are highly stretched. For example, the longest Si−Si bonds in the screw-dislocated NW containing six cross-sectional {111} planes are 2.60 Å, compared to a pristine bond length of 2.35 Å.

TABLE 2. Geometric Characteristics, Energetics, and Band Gaps of the DFTB Relaxed Screw-Dislocated ZnO (*L*,*h*) NWs and NTs[a]

$(L,h)_b$	$\|T_E\|$ (Å)	ε (%)	θ_E (deg)	γ_E (deg/Å)	E_d (eV/Å)	band gap (eV)
$(2,0)_b$	5.32	0.1	14.3	2.69	0.80	2.55
$(3,0)_b$	5.32	0.2	6.7	1.26	1.13	2.58
$(3,1)_b$	5.37	1.1	6.4	1.19	0.17	3.27
$(3,0)_b$[b]	5.28	−0.8				0.81 (1.0[c])
$(3,1)_b$[b]	5.29	−0.6				1.33 (2.06[c])
$(4,0)_b$	5.33	0.2	3.8	0.72	1.35	2.62
$(4,1)_b$	5.35	0.7	3.7	0.68	0.34	3.23
$(4,2)_b$	5.41	1.9	3.1	0.57	0.05	3.32
$(4,0)_b$[b]	5.32	0.2				0.56
$(3,1)_{3b}$	5.01	−5.8	16.0	3.20	1.32	3.01
$(4,1)_{3b}$	5.10	−4.1	10.3	2.02	2.97	2.39
$(4,2)_{3b}$	5.23	−1.6	8.7	1.66	0.45	3.24

[a] The magnitude of the dislocation is indicated in the subscript notation. Dislocation energy E_d is defined as the formation energy of the screw-dislocated structure minus the formation energy of the pristine one. [b] Results obtained with DFT. [c] These band gap values were obtained with LDA+U.

We now examine the consequences of the screw dislocation on the electronic properties, focusing on the fundamental band gap, Figure 2. All pristine NWs and NTs present direct band gaps with values consistent with the values in bulk material. Bulk Si has an indirect band gap. The pristine Si NWs have direct band gaps, a feature observed before in ⟨100⟩, ⟨110⟩, and ⟨111⟩ Si NWs[20,22] and that can be rationalized by considering the quantum confinement effect and simple band-folding arguments.[20] In Figure 2c, the quantum confinement effect is visible in the band gap decrease with size. The results summarized in Figure 2a and c evidence considerable downshifts in the band gaps of screw-dislocated NWs, which persist at all considered diameters. Extrapolation of the obtained monotonic dependence suggests that these differences are well maintained at larger *L*. In ZnO NTs, the band gap shifts are correlated with the wall thickness and size of the Burgers vector, Figure 2b, and are more significant in thick (*L*,*h*) NTs with large Burgers vector. Unlike in carbon NTs,[42] here we observe that the shear strain stored in the ZnO NT walls modifies the band gap very little.

More insight into this notable behavior can be gained by inspecting the band structures displayed in Figure 3. Responsible for the band gap decreases are

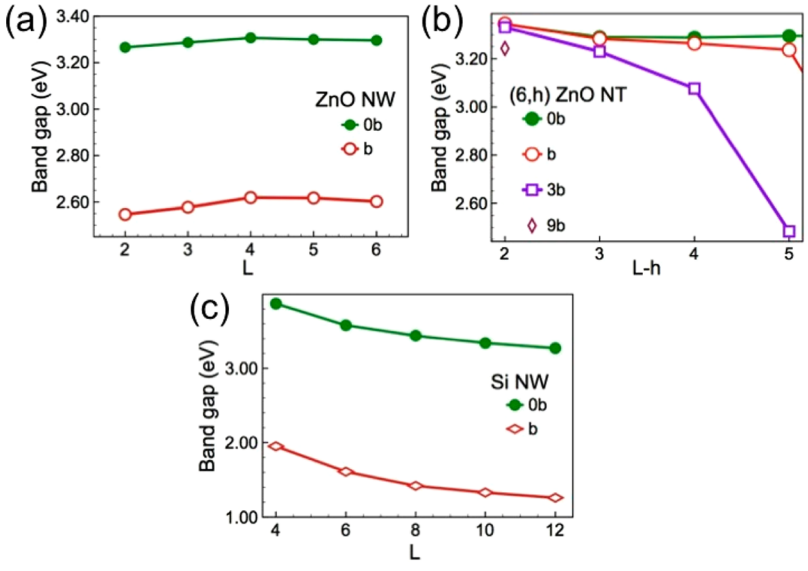

Figure 2. DFTB band gap variations with number of layers *L* in stress-free pristine and screw-dislocated (a) ZnO NWs, (b) ZnO NTs, and (c) Si NWs. Panel (b) shows the DFTB band gap variations with wall thickness, as measured by *L*−*h*, and Burgers vector size, in (6,*h*) ZnO NTs.

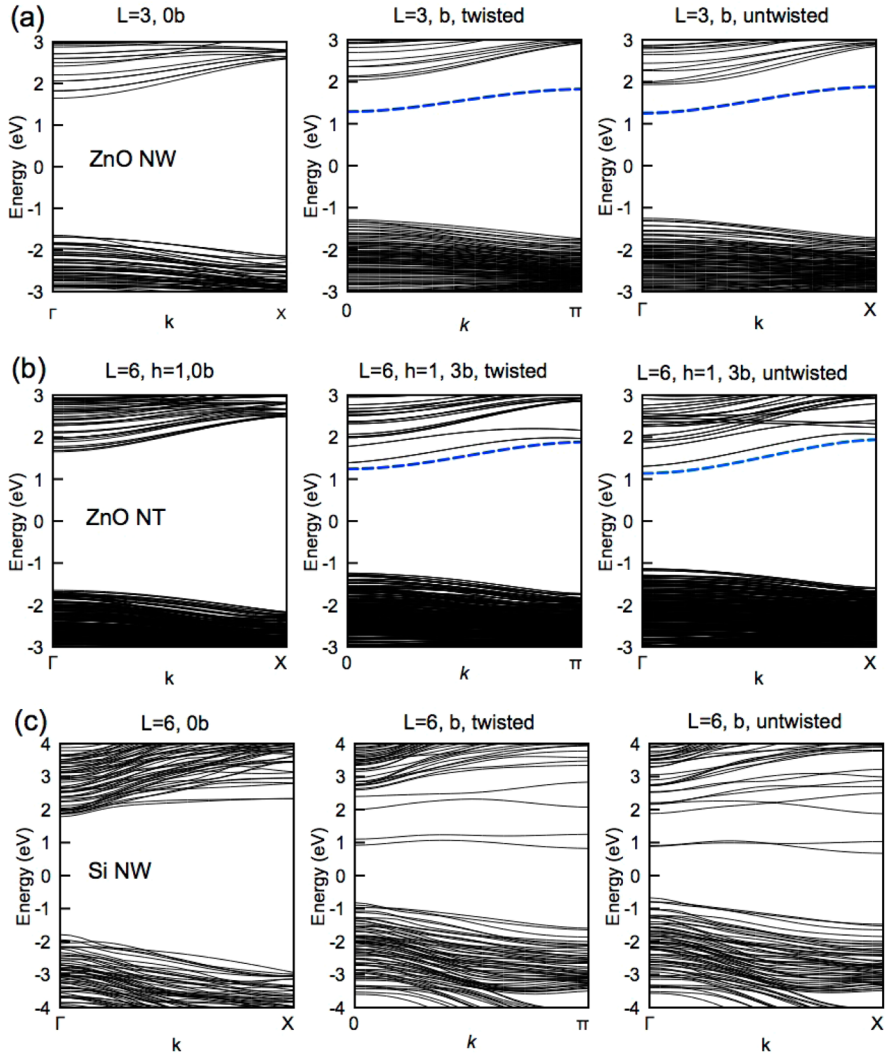

Figure 3. DFTB band structures for pristine (left) and screw-dislocated (center and right) (a) (3,0) ZnO NW, (b) (6,1) ZnO NT, and (c) (6,0) Si NW. Zero energy corresponds to the Fermi level set to the middle of the band gap. Dashed blue lines indicate the gap states developed in the screw-dislocated NWs.

the new gap states developed in the screw-dislocated NWs and NTs (see the dashed line in Figure 3a and b). As the number of atoms per computational cell in the screw-dislocated and pristine counterpart structures is the same, the gap states cannot be related to an extra number of electrons. Notably, even in the presence of the quantum confinement effect, all band gaps are indirect in screw-dislocated Si NWs, Figure 3c. An important observation is that the screw-dislocated but untwisted structures, Figure 3 (right), already display significant differences with their pristine partners, Figure 3 (left). The further occurrence of the Eshelby twist, Figure 3 (center), modifies the band gap very little in ZnO. In Si, the consequences of this symmetry-lowering deformation are clearly visible in the removal of many band degeneracies without leading to significant band gap changes. Overall, this analysis suggests that the core of the screw dislocation is the primary cause for the dramatic band gap modifications noted in Figure 2 and not the linear shear strain located outside the core region.

The effective coupling of the screw dislocation to the conduction states is visible in calculations carried out at higher levels of theory, such as the DFT calculations presented in Figure 4. Note that these calculations were performed under PBC, and thus the Eshelby twist effect (proved above to be less significant) is not captured. A comparison of DFT data with Figure 3a and c indicates that all the important features observed with DFTB, such as the singular band developed in the band gap of screw-dislocated ZnO NW, are still present in the DFT results. Furthermore, the additional plots of spatial wave function corresponding to the conduction band minimum evidence two causes for the observed band gap modifications: While in ZnO, the gap states are due to the new Zn−Zn interactions located in the core, in Si the lowering of the conduction band at the X point originates in the highly strained Hornstra core. This is in spite of the fact that all core atoms are still 4-fold coordinated. Note that this explanation is consistent with the DFTB result of Figure 3b. As mentioned

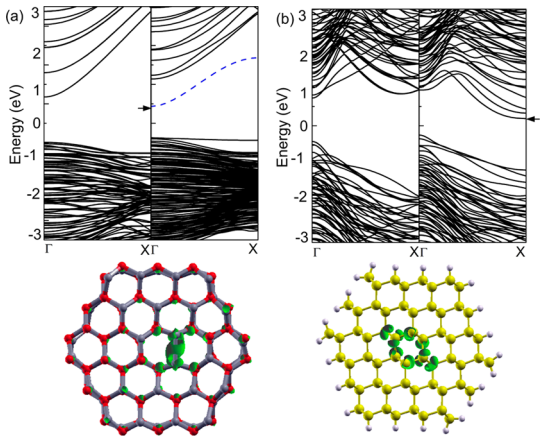

Figure 4. DFT band structures for pristine (left) and screw-dislocated (untwisted) (a) (3,0) ZnO NW and (b) (6,0) Si NW. The Fermi level is at the zero *y*-axis. To understand the mechanics of gap reduction, the spatial wave function distributions at the conduction band minimum of the dislocated structures (see arrows) are plotted underneath. The value of the isosurface (shown in green) was taken at 10% of the wave function maximum. Zn, O, Si, and H atoms are shown in gray, red, yellow, and light gray balls, respectively.

previously, although the (6,1) ZnO NT has a hollow core, the large Burgers vector leads to Zn−Zn interactions.

In agreement with previous reports,[20,23] our DFT calculations are underestimating the band gap of ZnO and Si nanostructures. For example, DFT gives a value of 1.17 eV for pristine (3,0) ZnO NW, about 3 times less than the semiempirical DFTB result. Note that the larger than bulk DFT band gap value is caused by the confinement effect.[23] Nevertheless, follow-up single-point LDA+U calculations based on the DFT relaxed geometries calculations summarized in the last columns of Tables 1 and 2 give more realistic band gap predictions. Most importantly, the LDA+U band structures are in agreement with the DFTB and DFT ones in all the important aspects (see for example the band structures shown in Figure S1 and Figure 4a). Thus, they confirm our DFTB findings.

CONCLUSIONS

We identified screw-dislocation band gap narrowing, an effect common to ZnO and Si nanomaterials. By carefully analyzing the relaxed structures and electronic properties, we traced this effect to the new homoelemental Zn−Zn interactions created in the screw-dislocated ZnO core and to the conduction band lowering at the X point caused by the highly strained Hornstra core of Si NWs. These newly identified mechanisms act independently from the known quantum confinement effects and should be present in nanostructures with diameters larger than the ones considered here as well as in similar nanostructures made out of other materials. In ZnO NTs, the band gap appears stable against the shear strain generated by the dislocation in the NT walls. Nevertheless, the band gap modulation effect is still present in thick NTs with large Burgers vectors, due to the same Zn−Zn interactions located in the small open cores.

We emphasize that the effect reported here is robust. The analyzed dislocation cores are already relaxed, and thus the band gap narrowing cannot be easily removed *via* dangling bond reconstruction. Furthermore, although the Eshelby twist has a negligible impact on the band gap, it plays an important role in stabilizing the dislocation at the center of the nanostructures.[37,38] Thus, the screw-dislocated NWs and NTs cannot easily heal. It was recently proposed[37] that the structural stability of synthesized screw-dislocated NW and NTs can be understood by analyzing the energetic costs for creating internal surfaces within the host NW *versus* the energy of the highly stained core dislocation region. This understanding, combined with the band gap dependences on the size of the Burgers vector and wall thickness observed here, could motivate new strategies for growing nanostructures with desired band gaps.

METHODS

In our DFTB calculations, we used an atomic basis comprised of sp basis functions for Si and O, spd for Zn, and s for H. For all structural relaxation calculations 10 *k* points were used and the energy relaxation threshold was set to 10^{-6} hartree. Static configuration band-structure calculations were performed with 45 *k* points. The DFTB parametrization predicts the structural properties of ZnO materials well, but it overestimates the band gap values in comparison with experimental data. That is why one of the parameters that refers to the on-site energy for the 4s electron of Zn was slightly changed from −0.2079 au to −0.3527 au in order to regain the experimentally measured band gap of the bulk wurtzite ZnO phase. Note that the larger DFTB band gaps compared to DFT are mainly due to error cancelation due to the minimal basis. The primitive domain placed under the objective boundary conditions (1) contains $N = 12(L^2 - h^2)$ atoms in both pristine and screw-dislocated (L,h) ZnO structures. Consideration of angular $(2\pi/3)$ and helical $(\pi/3)$ symmetries leads to 6 times reduction in the cell size of the pristine structures. Taking into account angular symmetry in screw-dislocated NTs, the objective domains become 2 and 6 times smaller for $(L,h)_b$ and $(L,h)_{3b}$ NTs, respectively, than the original PBC cell size. Note that the forms of the objective boundaries and symmetry-adapted basis should be slightly changed, as discussed in ref 16. In our atomistic calculations, the smallest possible simulation domains were used in ZnO structures. In $(L,0)$ Si NWs, the computational domain comprises $4[(3/8)L^2 + (1/4)L]$ Si atoms and $4L$ H atoms. For a ball-and-stick representation of selected computational domains see Figure S3.

In our supporting DFT calculations, structural relaxation calculations were carried out with the linear combination of atomic orbital basis implemented in the SIESTA package,[43] using the Perdew−Burke−Ernzerh generalized gradient approximation for the exchange−correlation energy and norm-conserving pseudopotentials for the core−valence interactions.[44] The d electronic states of Zn were treated as valence states. The NW and NT structures were placed under PBC in all three dimensions separated by a vacuum region larger than 10 Å in radial

directions, so that the interaction with the image structures is negligible. The double-ζ polarized numerical atomic-orbital basis sets for all atoms were used. A $1 \times 1 \times 10$ Monkhorst–Pack k-point grid was used in the energy calculations. An energy cutoff of 300 Ry is sufficient to converge the grid integration of the charge density, and atomic positions are fully relaxed using a conjugate gradient method so that the force on each atom is less than 0.02 eV/Å. The single-point LDA+U calculations in ZnO were performed with the plane-wave-based Vienna *ab initio* package.[45] The electron wave functions were described using the projector-augmented wave method.[46] Plane waves have been included up to an energetic cutoff of 430 eV. For integration within the Brillouin zone, specific k points were selected using a $1 \times 1 \times 5$ Monckhorst–Pack grid. To improve the accuracy of the band gap result, we introduced a Coulomb energy parameter of 7 eV for the d orbital of Zn.[47,48] This value is in agreement with photoemission experiments. For the bulk wurtzite ZnO phase, the LDA+U gives a direct band gap[48] of 1.38 eV, which is larger than the 0.7 eV obtained by the DFT method, but still lower than the experimental 3.4 eV value.

Conflict of Interest: The authors declare no competing financial interest.

Acknowledgment. We acknowledge useful discussions with G. Seifert and A. de la Rosa. Work was supported by the NSF CAREER Grant CMMI-0747684. L.K. acknowledges financial support from the Alexander von Humboldt Foundation, Germany. Computations were carried out at the Minnesota Supercomputing Institute.

Supporting Information Available: The band structures of (3,0) and $(3,0)_b$ ZnO NWs calculated with LDA+U and of (4,0) and $(4,0)_b$ ZnO NWs calculated with DFT are shown in Figures S1 and S2, respectively. Figure S3 shows examples of objective domains used to simulate screw-dislocated ZnO and Si NWs. This material is available free of charge *via* the Internet at http://pubs.acs.org.

REFERENCES AND NOTES

1. Bierman, M. J.; Albert Lau, Y. K.; Kvit, A. V.; Schmitt, A. L.; Jin, S. Dislocation-Driven Nanowire Growth and Eshelby Twist. *Science* **2008**, *320*, 1060–1063.
2. Albert Lau, Y. K.; Chernak, D. J.; Bierman, M. J.; Jin, S. Formation of PbS Nanowire Pine Trees Driven by Screw Dislocations. *J. Am. Chem. Soc.* **2009**, *131*, 16461–16471.
3. Jacobs, B. W.; Crimp, M. A.; McElroy, K.; Ayres, V. M. Nanopipes in Gallium Nitride Nanowires and Nanorods. *Nano Lett.* **2008**, *8*, 4353–4358.
4. Zhu, J.; Peng, H.; Marshall, A. F.; Barnett, D. M.; Nix, W. D.; Cui, Y. Formation of Chiral Branched Nanowires by the Eshelby Twist. *Nat. Nanotechnol.* **2008**, *3*, 477–481.
5. Morin, S. A.; Bierman, M. J.; Tong, J.; Jin, S. Mechanism and Kinetics of Spontaneous Nanotube Growth Driven by Screw Dislocations. *Science* **2010**, *328*, 476–480.
6. Morin, S. A.; Jin, S. Screw Dislocation-Driven Epitaxial Solution Growth of ZnO Nanowires Seeded by Dislocations in GaN Substrates. *Nano Lett.* **2010**, *10*, 3459–3463.
7. Tizei, L. H. G.; Craven, A. J.; Zagonel, L. F.; Tencé, M.; Stéphan, O.; Chiaramonte, T.; Cotta, M. A; Ugarte, D. Enhanced Eshelby Twist on Thin Wurtzite InP Nanowires and Measurement of Local Crystal Rotation. *Phys. Rev. Lett.* **2011**, *107*, 195503–1–195503–5.
8. Maestre, D.; Haussler, D.; Cremades, A.; Jager, W.; Piqueras, J. Complex Defect Structure in the Core of Sn-Doped In_2O_3 Nanorods and Its Relationship with a Dislocation-Driven Growth Mechanism. *J. Phys. Chem. C* **2011**, *115*, 18083–18087.
9. Hacialioglu, S.; Meng, F.; Jin, S. Facile and Mild Solution Synthesis of Cu_2O Nanowires and Nanotubes Driven by Screw Dislocations. *Chem. Commun.* **2012**, *48*, 1174–1176.
10. Wu, H.; Meng, F.; Li, L.; Jin, S.; Zheng, G. Dislocation-Driven CdS and CdSe Nanowire Growth. *ACS Nano* **2012**, *6*, 4461–4468.
11. Eshelby, J. D. Screw Dislocations in Thin Rods. *J. Appl. Phys.* **1952**, *24*, 176–179.
12. Eshelby, J. D. The Twist in a Crystal Whisker Containing a Dislocation. *Philos. Mag.* **1958**, *3*, 440–447.
13. Yoshida, K. Twists and Hollow Dislocations in KCl Tubular Whiskers. *Jpn. J. Appl. Phys.* **1964**, *3*, 565–571.
14. Dumitrică, T.; James, R. D. Objective Molecular Dynamics. *J. Mech. Phys. Sol.* **2007**, *55*, 2206–2236.
15. James, R. D. Objective Structures. *J. Mech. Phys. Sol.* **2006**, *54*, 2354–2390.
16. Zhang, D.-B.; Hua, M.; Dumitrică, T. Stability of Polycrystalline and Wurtzite Si Nanowires *via* Symmetry-Adapted Tight-Binding Objective Molecular Dynamics. *J. Chem. Phys.* **2008**, *128*, 084104-1–084104-9.
17. Rurali, R.; Hernandez, E. Trocadero: A Multiple-Algorithm Multiple-Model Atomistic Simulation Program. *Comput. Mater. Sci.* **2003**, *28*, 85–106.
18. Moreira, N. H.; Dolgonos, G.; Aradi, B.; Rosa, A. L.; Frauenheim, Th. Toward an Accurate Density-Functional Tight-Binding Description of Zinc-Containing Compounds. *J. Chem. Theory Comput.* **2009**, *5*, 605–614.
19. Frauenheim, Th.; Weich, F.; Kohler, Th.; Uhlmann, S.; Porezag, D.; Seifert, G. Density-Functional-Based Construction of Transferable Nonorthogonal Tight-Binding Potentials for Si and SiH. *Phys. Rev. B* **2005**, *52*, 11492–11501.
20. Yan, J.-A.; Yang, L.; Chou, M. Y. Size and Orientation Dependence in the Electronic Properties of Silicon Nanowires. *Phys. Rev. B* **2007**, *76*, 115319–1–115319–6.
21. Erwin, S. C.; Zu, L.; Haftel, M. I.; Efros, Al.L.; Kennedy, T. A.; Norris, D. J. Doping Semiconductor Nanocrystals. *Nature* **2005**, *436*, 91–94.
22. Nolan, M.; Sean O'Callaghan, S.; Fagas, G.; Greer, J. C.; Frauenheim, Th. Silicon Nanowire Band Gap Modification. *Nano Lett.* **2007**, *7*, 34–38.
23. Pan, H.; Feng, Y. P. Semiconductor Nanowires and Nanotubes: Effects of Size and Surface-to-Volume Ratio. *ACS Nano* **2008**, *2*, 2410–2414.
24. Guo, C. S.; Luo, L. B.; Yuan, G. D.; Yang, X. B.; Zhang, R. Q.; Zhang, W. J.; Lee, S. T. Surface Passivation and Transfer Doping of Silicon Nanowires. *Angew. Chem., Int. Ed.* **2009**, *121*, 10080–10084.
25. Yang, Y.; Yan, X. H.; Xiao, Y.; Lu, D. Size-Dependent Strain Effects on Electronic and Optical Properties of ZnO Nanowires. *Appl. Phys. Lett.* **2010**, *97*, 033106-1–033106-3.
26. Zhang, F.; Crespi, V. H.; Zhang, P. Prediction that Uniaxial Tension Along <111> Produces a Direct Band Gap in Germanium. *Phys. Rev. Lett.* **2009**, *102*, 156401–1–156401–4.
27. Huang, M.; Ritz, C. S.; Novakovic, B.; Yu, D.; Zhang, Y.; Flack, F.; Savage, D. E.; Evans, P. G.; Knezevic, I.; Liu, F.; *et al.* Mechano-Electronic Superlattices in Silicon Nanoribbons. *ACS Nano* **2009**, *3*, 721–727.
28. Sánchez-Pérez, J. R.; Boztug, C.; Chen, F.; Sudradjat, F. F.; Paskiewicz, D. M.; Jacobson, R. B.; Lagally, M. G.; Paiella, P. Direct-Bandgap Light-Emitting Germanium in Tensilely Strained Nanomembranes. *Proc. Natl. Acad. Sci. U. S. A.* **2011**, *108*, 18893–18898.
29. Huang, M. H.; Mao, S.; Feick, H.; Yan, H.; Wu, Y.; Kind, H.; Weber, E.; Russo, R.; Yang, P. Room-Temperature Ultraviolet Nanowire Nanolasers. *Science* **2001**, *292*, 1897–1899.
30. Garnett, E.; Yang, P. Light Trapping in Silicon Nanowire Solar Cells. *Nano Lett.* **2010**, *10*, 1082–1087.
31. Law, M.; Greene, L. E.; Johnson, J. C.; Saykally, R.; Yang, P. Nanowire Dye-Sensitized Solar Cells. *Nat. Mater.* **2005**, *4*, 455–459.
32. Matare, H. F. *Defect Electronics in Semiconductors*; Wiley-Interscience: New York, 1971.
33. Müller, E.; Gerthsen, D.; Brückner, P.; Scholz, F.; Gruber, Th.; Waag, A. Probing the Electrostatic Potential of Charged Dislocations in *n*-GaN and *n*-ZnO Epilayers by Transmission Electron Holography. *Phys. Rev. B* **2006**, *73*, 2453161-1–2453161-9.
34. Wander, A.; Harrison, N. M. An *Ab Initio* Study of ZnO $(10\bar{1}0)$. *Surf. Sci. Lett.* **2000**, *457*, L342–L346.
35. Wander, A.; Harrison, N. M. An *Ab Initio* Study of ZnO $(11\bar{2}0)$. *Surf. Sci. Lett.* **2000**, *468*, L851–L855.

36. Meyer, B.; Marx, D. Density-Functional Study of the Structure and Stability of ZnO Surfaces. *Phys. Rev. B* **2003**, *67*, 035403-1–035403-11.
37. Akatyeva, E.; Dumitrică, T. Eshelby Twist and Magic Helical Zinc Oxide Nanowires and Nanotubes. *Phys. Rev. Lett.* **2012**, *109*, 035501-1–035501-5.
38. Nikiforov, I.; Zhang, D.-B.; Dumitrică, T. Screw Dislocations in <110> Silicon Nanowires: An Objective Molecular Dynamics Study. *J. Phys. Chem. Lett.* **2011**, *2*, 2544–2548.
39. Zhang, D.-B.; James, R. D.; Dumitrică, T. Dislocation Onset and Nearly Axial Glide in Carbon Nanotubes under Torsion. *J. Chem. Phys.* **2009**, *130*, 071101-1–071101-4.
40. Zhang, D.-B.; Dumitrică, T.; Seifert, G. Helical Nanotube Structures of MoS_2 with Intrinsic Twisting: An Objective Molecular Dynamics Study. *Phys. Rev. Lett.* **2010**, *104*, 065502-1–065502-4.
41. Zhang, D.-B.; Akatyeva, E.; Dumitrică, T. Helical BN and ZnO Nanotubes with Intrinsic Twisting: An Objective Molecular Dynamics Study. *Phys. Rev. B* **2011**, *84*, 115431-1–115431-8.
42. Zhang, D.-B.; James, R. D.; Dumitrică, T. Electromechanical Characterization of Carbon Nanotubes in Torsion *via* Symmetry Adapted Tight-Binding Objective Molecular Dynamics. *Phys. Rev. B* **2009**, *80*, 115418-1–115418-5.
43. Soler, J. M.; Artacho, E.; Gale, J. D.; García, A.; Junquera, J.; Ordejón, P.; Sánchez-Portal, D. The SIESTA Method for *Ab Initio* Order-N Materials Simulation. *J. Phys.: Condens. Matter* **2002**, *14*, 2745–2779.
44. Perdew, J. P.; Burke, K.; Ernzerhof, M. Generalized Gradient Approximation Made Simple. *Phys. Rev. Lett.* **1996**, *77*, 3865–3868.
45. Kresse, G.; Joubert, D. From Ultrasoft Pseudopotentials to the Projector Augmented-Wave Method. *Phys. Rev. B* **1999**, *59*, 1758–1775.
46. Blöchl, P. E. Projector Augmented-Wave Method. *Phys. Rev. B* **1994**, *50*, 17953–17979.
47. Lany, S.; Zunger, A. Anion Vacancies as a Source of Persistent Photoconductivity in II-VI and Chalcopyrite Semiconductors. *Phys. Rev. B* **2005**, *72*, 035215-1–035215-13.
48. Lany, S.; Zunger, A. Assessment of Correction Methods for the Band-Gap Problem and for Finite-Size Effects in Supercell Defect Calculations: Case Studies for ZnO and GaAs. *Phys. Rev. B* **2008**, *78*, 235104-1–235104-25.